Environmental Science and Pollution Research (2023) 30:92611–92620
https://doi.org/10.1007/s11356-023-28804-2

RESEARCH ARTICLE

Improving water treatment using a novel antibacterial kappa-carrageenan–coated magnetite decorated with silver nanoparticles

Ali Seraj[1] · Alireza Allafchian[2,3] · Fathallah Karimzadeh[1,2] · Arian Valikhani[1] · Seyed Amir Hossein Jalali[3,4]

Received: 29 April 2023 / Accepted: 11 July 2023 / Published online: 26 July 2023

Abstract

In this study, we aimed to fabricate an enhanced antibacterial agent to act against pathogenic bacteria in aqueous environments. To achieve this, silver nanoparticles (AgNPs) were inlaid on a kappa-carrageenan (KC) base and coated on Fe_3O_4 magnetic cores (Fe_3O_4@KC@Ag). Superparamagnetic Fe_3O_4 nanoparticles were designed at the center of the composite nanostructure, allowing magnetic recovery from aqueous media in the presence of a magnet. The synthesized nanoconjugate was characterized in each step using XRD, FT-IR, EDX, FE-SEM, TEM, DLS, VSM, and disk-diffusion antibacterial method. Results show that the nanocomposite system is formed, while the magnetic properties remain practically stable. The agglomeration of the AgNPs was decreased by the trap-like function of KC coating, which resulted in an improved antibacterial activity for the Fe_3O_4@KC@Ag formulation. These findings suggest that Fe_3O_4@KC@Ag nanocomposites could be promising agents for combating bacterial infections in aqueous environments.

Keywords Water treatment · Kappa-carrageenan · Superparamagnetic nanoparticle · Silver nanoparticle · Antibacterial activity

Introduction

Potable water, which makes up only 2.5% of the Earth's total water, is essential for maintaining human health (Erukhimovich and Olvera de La Cruz 2007, Hillie and Hlophe 2007). However, rapid population growth has led to a water shortage, making purification a critical step in ensuring the availability of safe drinking water. Waterborne pathogens, including viruses, bacteria, helminths, and protozoa, can cause serious systematic and gastrointestinal diseases (Muoio, Caretti et al. 2020). Currently, water disinfection has primarily relied on processes such as ultraviolet irradiation, ozonation, chlorination, and chemical treatments like chloramine (Miao, Teng et al. 2019). These traditional methods, however, have limitations, including low durability, toxic byproducts, high cost, and low impact on viruses (Mukhopadhyay, Duttagupta et al. 2022). Therefore, alternative or complementary methods are necessary needs.

Nanotechnology has emerged as a promising field for developing solutions to fight pathogenic microorganisms. Nanoparticles (NPs), which have a high specific surface area and small size (typically below 100 nm), offer a high reactivity and have been shown to have antibacterial properties.

Highlights
- Rapid three-step synthesis of magnetic Fe_3O_4@kappa-carrageenan@Ag nanocomposite was fabricated.
- The presence of KC in the nanocomposite significantly enhanced the antibacterial function of AgNPs, resulting in a nanocomposite with a distinguishably higher bactericidal activity.
- Fe_3O_4@KC@Ag nanocomposite could be offer as an efficient and cost-effective platform for improving water treatment, which is a major public health concern worldwide.

Responsible Editor: Guilherme Luiz Dotto

✉ Alireza Allafchian
allafchian@iut.ac.ir

[1] Department of Materials Engineering, Isfahan University of Technology, 84156, Isfahan 83111, Iran

[2] Research Institute for Nanotechnology and Advanced Materials, Isfahan University of Technology, 84156, Isfahan 83111, Iran

[3] Research Institute for Biotechnology and Bioengineering, Isfahan University of Technology, 84156, Isfahan 83111, Iran

[4] Department of Natural Resources, Isfahan University of Technology, 84156, Isfahan 83111, Iran

Among them, silver nanoparticles (AgNPs) are widely studied due to their recognized antibacterial nature and ease of application (Amiri, Vatanpour et al. 2022, Yonathan, Mann et al. 2022).

In recent years, numerous publications have focused on the synthesis and characterization of AgNPs with antimicrobial properties. For instance, Rama et al. (2022) explored the production of antimicrobial, antioxidant, and angiogenic bioactive silver nanoparticles using Murraya paniculata (L.) jack leaves (Rama, Baldelli et al. 2022). Prabhu and Poulose (2012) discussed the mechanism of antimicrobial action, synthesis, medical applications, and toxicity effects of silver nanoparticles (Prabhu and Poulose 2012). Although the precise mechanism of bacterial death by nanoparticles is not firmly specified, it is believed that AgNPs attack bacteria by attaching and penetrating their membranes (Jalili, Allafchian et al. 2019). Dakal et al. (2016) focused on the mechanistic basis of the antimicrobial actions of AgNPs, shedding light on the underlying mechanisms. They noted that the interaction between AgNPs and antibacterial agents, including the release of Ag^+ ions and subsequent reactions with cellular components, can result in the death or mutation of bacteria (Dakal, Kumar et al. 2016). It has been reported that smaller nanoparticles can exhibit greater antibacterial activity, but the agglomeration of AgNPs poses a challenging issue (Guzman, Dille et al. 2012). To address this problem and stabilize AgNPs, several techniques have been employed, such as immobilization on polymeric platforms, which minimizes the toxicity of AgNPs (Zahran and Marei 2019, Zhao, Tian et al. 2022).

In this study, we focus on the utilization of kappa-carrageenan (KC), an environmentally friendly polymer (Fig. 1) that is known as a sulfated polysaccharide and a member of the carrageenan family (Abdullah, Azeman et al. 2018). Carrageenans are water-soluble biopolymers consisting of D-galactose residues connected intermittently in α-1, 3, and β-1, 4 bonds in addition to pyranosidic rings and are famous for their desirable gel-forming ability (Daniel-da-Silva, Fateixa et al. 2009, Jiang, Zhang et al. 2021). They have been mainly applied in food, cosmetics, and pharmaceutical industries as stabilizing, emulsifying, and gelificant agents. KC, obtained from a red marine algae by the name of *Rhodophyceae*, is a non-toxic water-soluble polymer that can form a thermoreversible gel (Şen and Erboz 2010, Prasetyaningrum and Praptyana 2019). In addition, KC products such as oligosaccharides show a sensible bactericidal activity (Wang, Yao et al. 2012). Therefore, as a natural carbohydrate, KC could act in synergy with AgNPs against bacteria.

On the other hand, the presence of a magnetic core at the center of these particles can significantly facilitate their separation from aqueous media and provides a chance of recycling them for the next treatment cycles (Lin, Cui et al. 2013, Allafchian, Jalali et al. 2016). Aside from applications in drug delivery (Nikforouz, Allafchian et al. 2021), hyperthermia (Yang, Huang et al. 2020), catalysis(Li, Zhao et al. 2019), and magnetic resonance imaging (MRI) (Wu, Sun et al. 2019, Yu, Zhao et al. 2019), superparamagnetic Fe_3O_4 NPs can play an important role as the core of a nanocomposite structure for water treatment processes. One research group studied the synthesis and characterization of a hydrogel called kappa-carrageenan grafted with N-hydroxyethylacrylamide (κC-*g*-PHEAA) (κC-g-PHEAA) and a hybrid nanocomposite containing Fe_3O_4 nanoparticles (Kulal and Badalamoole 2020). The nanocomposite displayed superparamagnetic behavior and both the hydrogel and nanocomposite exhibited high adsorption capacity for cationic dyes and metal ions in aqueous solutions. The presence of magnetite nanoparticles improved adsorption and enabled easy separation using an external magnetic field (Kulal and Badalamoole 2020). These findings suggest that the synthesized adsorbents hold promise for effective removal of dyes and metal ions from wastewater.

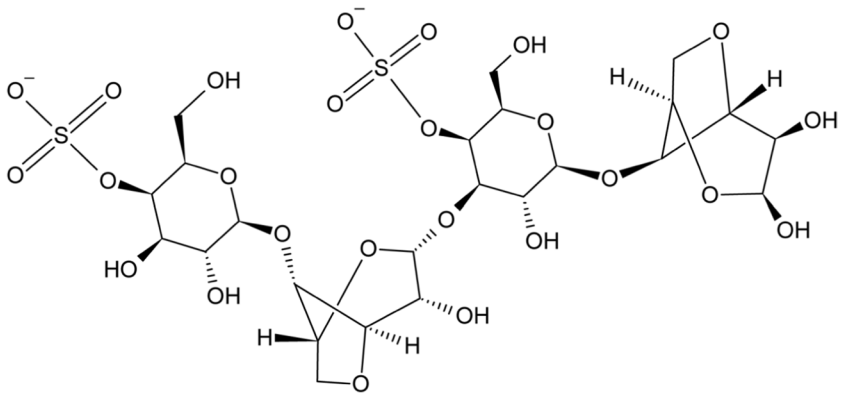

Fig. 1 The chemical structure of κ-carrageenan

In this study, we aimed to synthesize and characterize a novel Fe_3O_4@KC@Ag nanocomposite with efficient antibacterial activity. While the antibacterial properties of AgNPs have been widely studied, the use of KC as a synergistic agent in conjunction with AgNPs to combat bacteria is relatively novel and less explored in the literature. We aimed to investigate the combined antimicrobial efficacy of AgNPs and KC and explore the potential of this synergistic approach for water disinfection. By utilizing KC as a stabilizing agent for AgNPs and evaluating their combined effects, we also aimed to enhance the antimicrobial activity and stability of AgNPs, thus providing a novel approach to address the challenges associated with traditional water disinfection methods. Furthermore, our study incorporates the incorporation of a magnetic core, superparamagnetic Fe_3O_4 nanoparticles, in the nanocomposite structure. This magnetic core not only facilitates the separation of the nanocomposite from aqueous media but also opens up possibilities for their reuse in subsequent treatment cycles. Findings indicated that the Fe_3O_4 core at the center of the particles can significantly facilitate their separation from aqueous media and also the final nanocomposite depicted reliable antibacterial performance against both Gram-negative and Gram-positive bacteria.

Method

Materials and instruments

All chemicals in this research were of analytical grade and were used without further purification. The precursors including KC, ferric chloride hexahydrate ($FeCl_3.6H_2O$, ≥99%), ferrous chloride tetrahydrate ($FeCl_2.4H_2O$, ≥99.0%), sodium hydroxide (NaOH, ≥98%), silver nitrate ($AgNO_3$, ≥99.0%) and hydrazine (N_2H_4, 98%) were purchased from Merck (Germany). All solutions were prepared with double distilled water as solvent. XRD patterns were obtained by a Philips X-ray diffractometer using Cu-Kα radiation in the range of 10.02 to 99.97° (35 kV, 20 mA). The FT-IR tests were carried out using a Jasco spectrophotometer, and FE-SEM images were taken using a Hitachi S4160 device. A thin layer of gold was sputter coated on the samples before taking the FE-SEM images. The morphology of the nanocomposite was explored in detail by TEM (Philips CM10-HT), and the hydrodynamic diameter of the particles was measured by DLS (Horiba SZ-100). The magnetic nature of the samples was investigated by VSM (Danesh Pajoh).

Synthesis of Fe_3O_4 cores

Fe_3O_4 nanoparticles were synthesized based on a co-precipitation method (Saxena and Singh 2017). To begin with, both $FeCl_3.6H_2O$ and $FeCl_2.4H_2O$ solutions (0.1 M) were independently prepared using 25 mL of distilled water. The solutions were mixer under an argon atmosphere at 60 °C. After 5 min stirring, NaOH solution (1 M) was added to the reaction container for a reduction process. Maintaining a temperature of 70 °C for 30 min was adequate to reach Fe_3O_4 black products. The chemical reaction presented in Eq. (1) illustrates the formation of magnetite nanoparticles (Petcharoen and Sirivat 2012, Marimón-Bolívar and González 2018).

$$2Fe^{3+} + Fe^{2+} + 8OH^- \rightarrow Fe_3O_4 + 4H_2O \quad (1)$$

The reaction vessel was cooled in ambient temperature; then, Fe_3O_4 NPs were separated and washed five times using a magnet. The particles were still moist, so they were kept in oven for 3 h at 80 °C to dry completely.

KC coating on the magnetite cores

As reported previously in coating Fe_3O_4 NPs with basil seed mucilage (Rayegan, Allafchian et al. 2018), a similar method was adopted for applying a layer of KC on them. Initially, 200 mg dried Fe_3O_4 was dispersed in 50 mL distilled water using an ultrasonic homogenizer at 150 W power for 10 min. After obtaining a 4 mg mL^{-1} homogeneous product, 120 mg KC powder was added to the solution. Here again, the ultrasonic homogenizer was used for 10 min; however, with 200 W power, this time not only for dispersing but also for coating KC powder on Fe_3O_4 NPs, which is achieved by many collisions between them. In the next step, separation was performed by a strong magnet, and afterwards, the coated NPs were oven dried for 16 h at 30 °C. Finally, mortar and pestle were used to grind the materials and obtain a smooth powder for further experiments.

Immobilizing of AgNPs on the Fe_3O_4@KC

AgNPs were simultaneously synthesized and stabilized on the KC base by applying a chemical reaction (Pandey, Do et al. 2020, Wan, Li et al. 2021). The KC-coated Fe_3O_4 NPs (155 mg) were dispersed in 10 mL $AgNO_3$ solution (0.2 M) using 200 W sonication for 10 min. Then, 10 mL of hydrazine (0.4 M) was added to the homogeneous solution as a reducing agent, while stirring by a mechanical paddle (500 rpm). This reaction, as shown in Eq. (2), took 30 min to be completed (Nickel, zu Castell et al. 2000).

$$4Ag^+ + N_2H_4 \rightarrow 4Ag + N_2 + 4H^+ \quad (2)$$

Finally, the Fe_3O_4@KC@Ag nanocomposites were obtained and separated using a magnet, then dried in an oven for 3 h at 40 °C.

Antibacterial tests

The antibacterial disk diffusion tests were carried out using four Gram-positive and Gram-negative strains of *S. aureus* (ATCC 29213), *B. cereus* (ATCC 14579), *S. typhimurium* (ATCC 14028), and *E. coli* (ATCC 35218). The bacterial suspension samples were prepared based on the 0.5 McFarland protocol and cultured in agar media. The nanoparticle samples were dispersed in sterile DI water and the disks saturated by the samples were introduced into the agar plates and incubated in 5% CO_2 atmosphere overnight. The $AgNO_3$ disks were considered as positive control and the corresponding disks of Fe_3O_4, KC, Fe_3O_4@KC, and Fe_3O_4@KC@Ag were tested. Finally, the plates were incubated at 37 °C for 24 h, and the diameters of the inhibition zones were measured. The obtained antibacterial inhibition zones around each disk were measured and reported for each sample. This test was repeated three times.

Results and discussion

Characterization study

XRD analysis

The XRD patterns of Fe_3O_4, KC, Fe_3O_4@KC, and Fe_3O_4@KC@Ag are shown in Fig. 2. As can be seen in the Fe_3O_4 pattern, ten peaks around 30.2°, 35.4°, 37.7°, 43.1°, 53.4°, 57.5°, 62.6°, 71.4°, 74.8°, and 75.3° are characterized corresponding to the (220), (311), (222), (400), (422), (511), (440), (620), (533), and (622) planes of the unit cell, respectively, matched with the standard JCPDS reference no. 65-3107. The average crystalline size of this inverse spinel structure, Fe_3O_4, was estimated to be 42 nm using the Scherrer equation. The KC pattern illustrates no peak, and it was expected due to polymeric nature of KC. Existence of a clear bulge, in addition to a set of reduced-intensity peaks in the Fe_3O_4@KC pattern, indicates a successful coating of KC over the magnetite. At last, in the Fe_3O_4@KC@Ag pattern, three added planes including (111), (200), and (311) at roughly 38°, 44°, and 77°, respectively, are in good accordance with JCPDS reference no. 4–783 database and verify attachment of AgNPs onto the polymeric base. All results were consistent with previous studies (Chudasama, Vala et al. 2009, He, Ma et al. 2013)

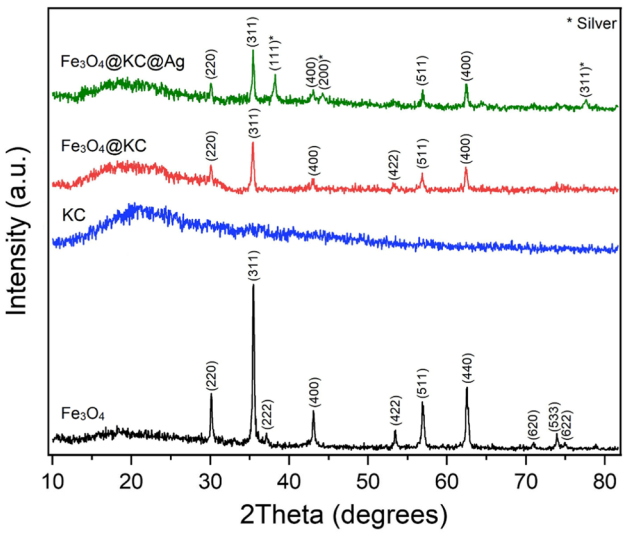

Fig. 2 XRD patterns of **a** Fe_3O_4, **b** KC, **c** Fe_3O_4@KC, and **d** Fe_3O_4@KC@Ag

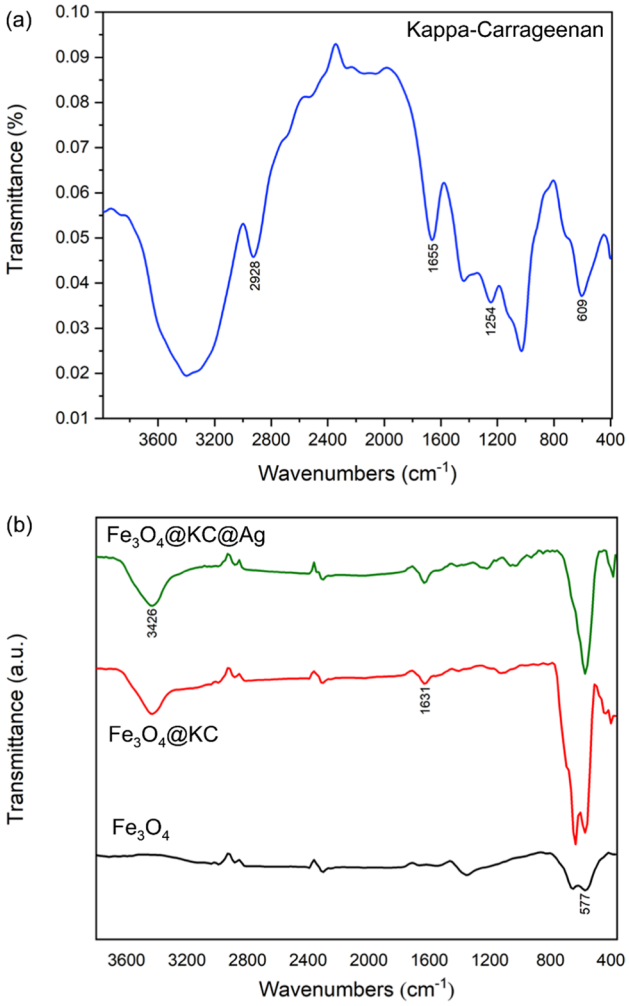

Fig. 3 **a** FT-IR spectrum of KC and **b** Fe_3O_4, Fe_3O_4@KC, and Fe_3O_4@KC@Ag

FT-IR spectroscopy

The FT-IR tests were carried out in the range of 4000–400 cm^{-1} at ambient temperature to explore the successful formation of coating and identify the functional groups. The infrared (IR) spectra of KC (Fig. 3a) exhibit characteristic bands corresponding to different functional groups. A broad band observed at 3400 cm^{-1} is assigned to the stretching vibrations of hydroxyl groups (–OH). Additionally, a sharp band at 1636 cm^{-1} is indicative of >C=O stretching. The bands observed at 1220 cm^{-1} and 846 cm^{-1} are attributed to the symmetric stretching vibration of O=S=O groups and the stretching vibration of –O–SO3 groups, respectively, which are associated with the substituted β–D–galactose residue. Another sharp and prominent band at 1023 cm^{-1} can be attributed to the glycosidic C–O–C vibration of the KC backbone. These spectral features provide valuable information about the presence and characteristic vibrations of various functional groups in KC (Şen and Erboz 2010). On the other hand, Fig. 3b shows the spectra of the prepared materials including Fe_3O_4, Fe_3O_4@KC, and Fe_3O_4@KC@Ag. As all three specimens are based on the magnetite NPs, an obvious similarity is expected among them. In case of magnetite, an important absorption band around 577 cm^{-1} is related to Fe–O stretching vibrations. Compared with magnetite, changes can be seen in Fe_3O_4@KC around 1631 cm^{-1} and in Fe_3O_4@KC@Ag around 3426 cm^{-1}, which correspond to –COO asymmetrical stretching of carboxylic groups and O=H (hydroxyl) groups, respectively (Allafchian, Jalali et al. 2017). This is considered as a proof of polymer coating on the magnetite NPs. Additionally, the broad peak observed in the FTIR spectra of Fe_3O_4@KC and Fe_3O_4@KC@Ag, located at approximately 3400 cm^{-1}, can be attributed to the presence of -OH groups in KC. Similarly, the peaks observed around 1220 cm^{-1} and 846 cm^{-1} provide confirmation of the presence of KC in the samples.

FE-SEM and TEM

FE-SEM and TEM were used to investigate the homogeneity and morphology of nanoparticles. FE-SEM images of magnetite, Fe_3O_4@KC, and Fe_3O_4@KC@Ag are shown in Fig. 4a–c. Evidently, all the particles are spherical and homogeneously distributed with the largest (126.22 ± 30.28 nm) and smallest (110.55 ± 26.28 nm) mean sizes belonging to Fe_3O_4@KC@Ag and Fe_3O_4@KC, respectively. Part of the reason why the addition of KC may result in a smaller mean size compared to Fe_3O_4 NPs could be attributed to the KC layer effectively preventing aggregation of Fe_3O_4 particles. Morphology and shape of nanoparticles are two key factors that directly affect their action and behavior in different media due to the influences on the physical, chemical, and magnetic properties of NPs (Mahmoudi, Sant et al. 2011, Alp and Aydogan 2016).

TEM image of the final nanocomposite allows demonstrating an illustration of the morphological details for the present components of magnetite, KC, and AgNPs that are distinguished by arrows based on the particle size results. As shown in Fig. 5a, almost all the black Fe_3O_4 NPs are trapped in the KC shell, while the gray AgNPs are attached to them. This thin layer of kappa-carrageenan acts as a support for Fe_3O_4 NPs and an anti-agglomeration agent for AgNPs. Thus, the bio-polymer KC can potentially improve the antibacterial function of AgNPs by increasing its contact surface with the surrounding pathogens.

EDX

EDX analysis was performed for assaying the element distribution on Fe_3O_4@KC@Ag nanocomposite. The analysis showed no sign of impurities in the spectrum as shown in Fig. 5b. A quantitative result from this test indicates that the nanocomposite includes 36.99% iron, 32.26% oxygen, 17.38% carbon, and 13.37% silver. This spectrum also shows that other materials, used in the synthesis process, were completely removed, and peaks around 2, 10, and 11.5 keV are due to the presence of Au that was used as a coated layer to perform the EDX test.

DLS

The prepared materials were tested by DLS to obtain their hydrodynamic particle size data. In Fig. 5c, the obtained DLS curves of Fe_3O_4, Fe_3O_4@KC, and Fe_3O_4@KC@Ag are illustrated. The Fe_3O_4 NPs had the polydispersity index (PDI) of 0.667 and a mean size of 445.8 nm. The PDI value ranges from 0 to 1, with zero referring to a perfectly monodispersed sample. There was a discrepancy between Fe_3O_4@KC and Fe_3O_4@KC@Ag as expected, and the mean sizes were 197.6 and 147.5 nm, respectively. Although it is expected that after each phase of the synthesis, the size of particles should be bigger. However, the data indicate opposite direction and are affected by a high agglomeration tendency of magnetite NPs. The more the layers are incorporated, the more dispersed the NPs are, and therefore, smaller particles are observed. Furthermore, PDI for magnetite coated KC and the final nanocomposite was 0.503 and 0.251, respectively.

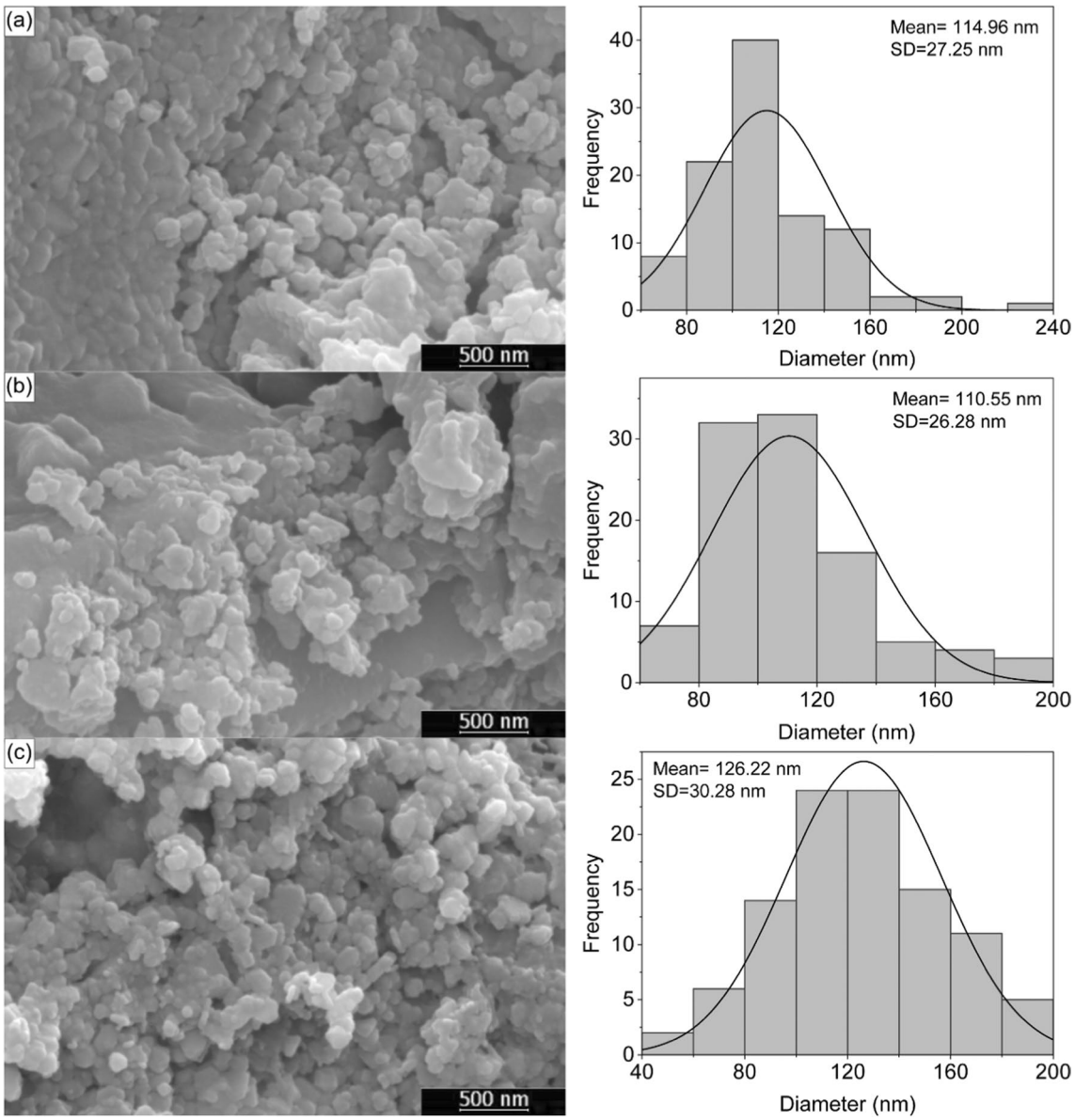

Fig. 4 FE-SEM images with particle size distributions of **a** Fe_3O_4, **b** Fe_3O_4@KC, and **c** Fe_3O_4@KC@Ag

Investigation of magnetic properties

The magnetic properties of the synthesized nanocomposite was assessed by VSM, and the results are depicted in Fig. 6 for Fe_3O_4, Fe_3O_4@KC, and Fe_3O_4@KC@Ag. The magnetic parameters including coercivity (H_c), saturated magnetization (M_s), and remnant magnetization (M_r) were determined and summarized in Table 1. It is observed that the attachment of non-magnetic materials, KC, and AgNPs, to the magnetic Fe_3O_4 leads to a decrease in the magnetic properties of the nanoparticles after each step of the fabrication process. However, it is noteworthy that the presence of KC on the magnetite is crucial for enhancing the antibacterial activity of AgNPs, and therefore, the reduction in magnetic properties should be considered as a trade-off. Despite the reduction, the final nanocomposite still exhibited a relatively high magnetic response, as shown in Fig. 6, indicating its potential for magnetic separation in wastewater and water treatment applications.

Evaluation of antibacterial activity

The bactericidal activity of Fe_3O_4@KC@Ag, Fe_3O_4@KC, Fe_3O_4, KC, and $AgNO_3$ against four bacterial strains, including two Gram-negative (*E. coli* and *S. typhimurium*) and two

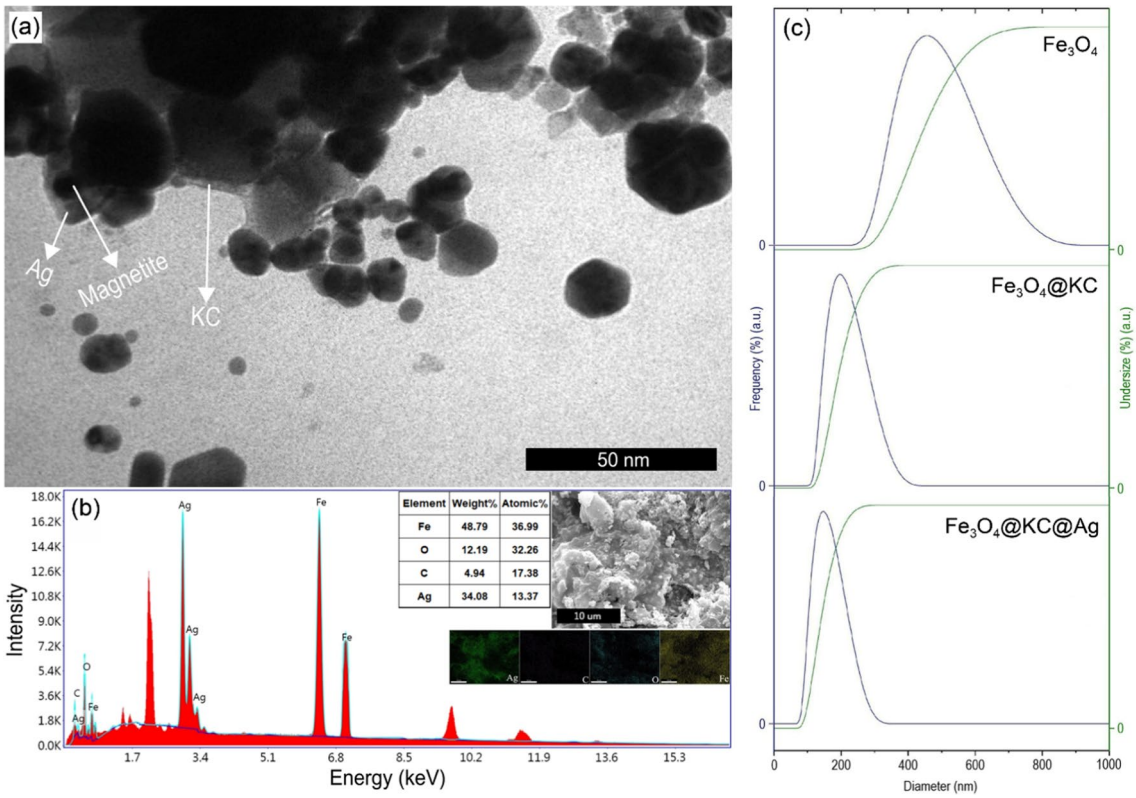

Fig. 5 **a** EDX spectrum and **b** elemental mapping of final nanocomposite (four main elements are illustrated with their subsequent fractions in the material). c Size distribution of Fe_3O_4, Fe_3O_4@KC, and Fe_3O_4@KC@Ag obtained by DLS

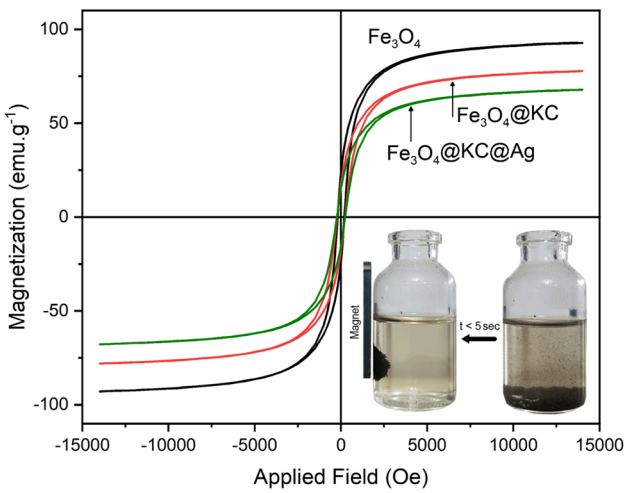

Fig. 6 Magnetization curves of Fe_3O_4, Fe_3O_4@KC, and Fe_3O_4@KC@Ag obtained by VSM in addition to a picture of nanocomposite behavior in presence of a magnet

Gram-positive (B. cereus and S. aureus), was evaluated by an agar diffusion test. The zones formed around the discs in this test called growth-inhibition zones, and the size of these zones reveals how well agents can combat infections. As seen in Fig. 7, the

Table 1 Magnetic parameters of the synthesized materials

Material	M_s (emu g^{-1})	M_r (emu g^{-1})	H_c (Oe)
Fe_3O_4	92.77	23.98	199.12
Fe_3O_4@KC	77.75	17.74	231.63
Fe_3O_4@KC@Ag	67.85	15.49	238.47

largest zones of inhibition were observed for the Fe_3O_4@KC@Ag sample for all four strains. Compared to AgNPs as a positive control, the Fe_3O_4@KC@Ag nanocomposite demonstrated superior antibacterial activity. The diameter of inhibition zones created around the samples (disks) were measured, and the results have been shown in Table 2. It is likely that the AgNPs embedded in the KC matrix contributed to the majority of the antibacterial effect, while KC alone did not significantly contribute to the inhibitory effect of the system. The stabilization of AgNPs onto the KC support might have controlled the release of AgNPs, resulting in higher antibacterial activity. The bactericidal effect of AgNPs is mainly attributed to the generation of reactive oxygen species (ROS), which can disrupt many vital processes for the viability of cells. ROS can cause cellular death either directly by inducing oxidative damage to the macromolecules of cells or indirectly by interfering with mechanisms such as autophagy.

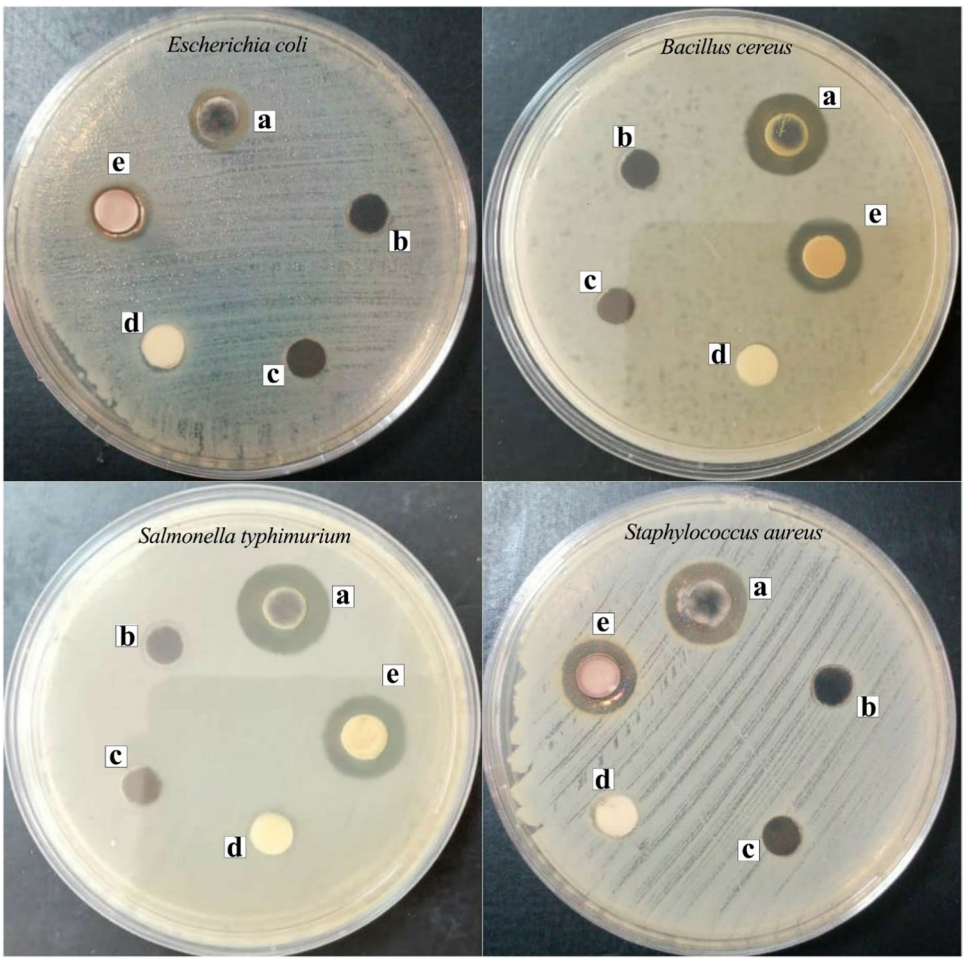

Fig. 7 Antibacterial activity of (a) Fe_3O_4@KC@Ag, (b) Fe_3O_4@KC, (c) Fe_3O_4, (d) KC, and (e) $AgNO_3$ demonstrated by inhibition zones

Table 2 Diameter of inhibition zones for synthesized materials and pure ones

Material	Inhibition zone ± 0.1 (mm)			
	E. coli	*S. typhimurium*	*B. cereus*	*S. aureus*
Fe_3O_4@KC@Ag	9.1	13.8	12.2	12.6
Fe_3O_4@KC	6.9	7.0	6.6	6.7
Fe_3O_4	6.4	6.4	6.4	6.4
KC	7.0	7.1	6.8	7.2
$AgNO_3$	7.9	12.4	11.3	11.3

Conclusions

Waterborne pathogens are a major public health concern worldwide due to their ability to cause a range of illnesses, from gastrointestinal ailments to serious systemic diseases. These microorganisms can contaminate drinking water sources, leading to infections in humans upon consumption or exposure. Therefore, it is necessary to develop efficient and cost-effective platforms for improving water treatment.

In this regard, here, the Fe_3O_4@KC@Ag nanocomposite was synthesized through a three-step procedure, and its successful coating of KC on the magnetite core and entrapping of AgNPs were confirmed through characterization studies. The polymeric base of the nanocomposite significantly upgraded the antibacterial function of AgNPS, as revealed by the disk diffusion method. The final nanocomposite exhibited a distinguishably higher bactericidal activity due to a reduction in the agglomeration tendency of AgNPs and optimization of their release. Furthermore, magnetic assessments indicated that all the structures could be easily separated from the medium. Hence, the Fe_3O_4@KC@Ag nanocomposite is a suitable candidate for wastewater and water treatment processes. Overall, the Fe_3O_4@KC@Ag nanocomposite has great potential as a water treatment material, and its development may lead to improved water quality and a reduction in waterborne illnesses. Future studies could explore its efficacy in removing other waterborne pathogens and assess its environmental impact.

Acknowledgements The authors wish to thank the Iranian Vice-President for Science and Technology and Research Institute for Biotechnology and Bioengineering for supporting this work.

Author contribution Ali Seraj: methodology, investigation, formal analysis, visualization, writing — original draft; Ali Reza Allafchian: project administration, supervision, conceptualization, writing — review and editing, resources; Fathallah Karimzadeh: supervision, conceptualization, writing — review and editing, resources; Arian Valikhani: methodology, investigation, formal analysis, visualization; Seyed Amir Hossein Jalali: supervision, conceptualization, writing — review and editing, resources.

Funding This work was supported by the Research Institute for Nanotechnology and Advanced Materials (RINAM) at Isfahan University of Technology, Iran.

Data availability The data and materials supporting the findings of this study are available upon reasonable request to the corresponding author.

Declarations

Ethics approval Not applicable

Consent to participate All participants provided written informed consent approved by the ethics committee. The informed consent form detailed the study purpose, procedures, risks, and benefits. By participating, participants agreed to the use of their data for research, including publication.

Consent for publication By submitting this manuscript, all authors explicitly agree to the publication of this manuscript in its current or revised form in any journal or other publication medium. All authors have reviewed and approved the final manuscript and have agreed to be accountable for all aspects of the work. All authors also confirm that this manuscript is original, has not been previously published, and is not under consideration for publication elsewhere.

Competing interests The authors declare no competing interests.

References

Abdullah S, Azeman NH, Mobarak NN, Zan MSD, Bakar AAA (2018) Sensitivity enhancement of localized SPR sensor towards Pb (II) ion detection using natural bio-polymer based carrageenan. Optik 168:784–793

Allafchian A, Jalali SAH, Bahramian H, Ahmadvand H (2016) 'Preparation, characterization, and antibacterial activity of $NiFe_2O_4$/PAMA/Ag–TiO_2 nanocomposite. J Magn Magn Mater 404:14–20

Allafchian A, Jalali SAH, Hosseini F, Massoud M (2017) Ocimum basilicum mucilage as a new green polymer support for silver in magnetic nanocomposites: production and characterization. J Environ Chem Eng 5(6):5912–5920

Alp E, Aydogan N (2016) A comparative study: synthesis of superparamagnetic iron oxide nanoparticles in air and N_2 atmosphere. Colloids Surf A Physicochem Eng Asp 510:205–212

Amiri S, Vatanpour V, Mansourpanah Y, Khataee A (2022) Recent trends in application of nanoscale zero-valent metals and metal single atoms in membrane processes. J Environ Chem Eng 10(3):107457

Chudasama B, Vala AK, Andhariya N, Upadhyay R, Mehta R (2009) Enhanced antibacterial activity of bifunctional Fe_3O_4-Ag core-shell nanostructures. Nano Res 2:955–965

Dakal TC, Kumar A, Majumdar RS, Yadav V (2016) Mechanistic basis of antimicrobial actions of silver nanoparticles. Front Microbiol 7:1831

Daniel-da-Silva AL, Fateixa S, Guiomar AJ, Costa BF, Silva NJ, Trindade T, Goodfellow BJ, Gil AM (2009) Biofunctionalized magnetic hydrogel nanospheres of magnetite and κ-carrageenan. Nanotechnology 20(35):355602

Erukhimovich I, Olvera de La Cruz M (2007) Phase equilibrium and charge fractionation in polyelectrolyte solutions. J Polym Sci B 45(21):3003–3009

Guzman M, Dille J, Godet S (2012) Synthesis and antibacterial activity of silver nanoparticles against gram-positive and gram-negative bacteria. Nanomed Nanotechnol Biol Med 8(1):37–45

He K, Ma F-X, Xu C-Y, Cumings J (2013) Mapping magnetic fields of Fe_3O_4 nanosphere assemblies by electron holography. J Appl Phys 113(17):17B528

Hillie T, Hlophe M (2007) Nanotechnology and the challenge of clean water. Nat Nanotechnol 2(11):663–664

Jalili MA, Allafchian A, Karimzadeh F, Nasiri F (2019) Synthesis and characterization of magnetite/Alyssum homolocarpum seed gum/Ag nanocomposite and determination of its antibacterial activity. Int J Biol Macromol 139:1263–1271

Jiang J-L, Zhang W-Z, Ni W-X, Shao J-W (2021) Insight on structure-property relationships of carrageenan from marine red algal: a review. Carbohydr Polym 257:117642

Kulal P, Badalamoole V (2020) Hybrid nanocomposite of kappa-carrageenan and magnetite as adsorbent material for water purification. Int J Biol Macromol 165:542–553

Li S, Zhao X, Yu X, Wan Y, Yin M, Zhang W, Cao B, Wang H (2019) Fe_3O_4 nanozymes with aptamer-tuned catalysis for selective colorimetric analysis of ATP in blood. Anal Chem 91(22):14737–14742

Lin L, Cui H, Zeng G, Chen M, Zhang H, Xu M, Shen X, Bortolini C, Dong M (2013) Ag–$CuFe_2O_4$ magnetic hollow fibers for recyclable antibacterial materials. J Mater Chem B 1(21):2719–2723

Mahmoudi M, Sant S, Wang B, Laurent S, Sen T (2011) Superparamagnetic iron oxide nanoparticles (SPIONs): development, surface modification and applications in chemotherapy. Adv Drug Deliv Rev 63(1-2):24–46

Marimón-Bolívar W, González EE (2018) Green synthesis with enhanced magnetization and life cycle assessment of Fe3O4 nanoparticles. Environ Nanotechnol Monit Manag 9:58–66

Miao H, Teng Z, Wang S, Xu L, Wang C, Chong H (2019) Recent advances in the disinfection of water using nanoscale antimicrobial materials. Adv Mater Technol 4(5):1800213

Mukhopadhyay A, Duttagupta S, Mukherjee A (2022) Emerging organic contaminants in global community drinking water sources and supply: a review of occurrences, processes and removal. J Environ Chem Eng 10(3):107560

Muoio R, Caretti C, Rossi L, Santianni D, Lubello C (2020) Water safety plans and risk assessment: a novel procedure applied to treated water turbidity and gastrointestinal diseases. Int J Hyg Environ Health 223(1):281–288

Nickel U, Castell AZ, Pöppl K, Schneider S (2000) A silver colloid produced by reduction with hydrazine as support for highly sensitive surface-enhanced Raman spectroscopy. Langmuir 16(23):9087–9091

Nikforouz B, Allafchian A, Jalali SAH, Shakeripour H, Mohammadinezhad R (2021) Quince seed mucilage coated iron oxide nanoparticles for plasmid DNA delivery. Nanotechnology 33(7):075102

Pandey S, Do JY, Kim J, Kang M (2020) Fast and highly efficient catalytic degradation of dyes using κ-carrageenan stabilized silver nanoparticles nanocatalyst. Carbohydr Polym 230:115597

Petcharoen K, Sirivat A (2012) Synthesis and characterization of magnetite nanoparticles via the chemical co-precipitation method. Mater Sci Eng: B 177(5):421–427

Prabhu S, Poulose EK (2012) Silver nanoparticles: mechanism of antimicrobial action, synthesis, medical applications, and toxicity effects. Int Nano Lett 2:1–10

Prasetyaningrum A, Praptyana I (2019) Carrageenan: nutraceutical and functional food as future food. In: IOP Conference Series: Earth and Environmental Science. IOP Publishing

Rama P, Baldelli A, Vignesh A, Altemimi AB, Lakshmanan G, Selvam R, Arunagirinathan N, Murugesan K, Pratap-Singh A (2022) Antimicrobial, antioxidant, and angiogenic bioactive silver nanoparticles produced using Murraya paniculata (L.) jack leaves. Nanomater Nanotechnol 12

Rayegan A, Allafchian A, Sarsari IA, Kameli P (2018) Synthesis and characterization of basil seed mucilage coated Fe_3O_4 magnetic nanoparticles as a drug carrier for the controlled delivery of cephalexin. Int J Biol Macromol 113:317–328

Saxena N, Singh M (2017) Efficient synthesis of superparamagnetic magnetite nanoparticles under air for biomedical applications. J Magn Magn Mater 429:166–176

Şen M, Erboz EN (2010) Determination of critical gelation conditions of κ-carrageenan by viscosimetric and FT-IR analyses. Food Res Int 43(5):1361–1364

Wan H, Li C, Mahmud S, Liu H (2021) Kappa carrageenan reduced-stabilized colloidal silver nanoparticles for the degradation of toxic azo compounds. Colloids Surf A Physicochem Eng Asp 616:126325

Wang FF, Yao Z, Wu HG, Zhang SX, Zhu NN, Gai X (2012) Antibacterial activities of kappa-carrageenan oligosaccharides. Appl Mech Mater 108:194–199

Wu F, Sun B, Chu X, Zhang Q, She Z, Song S, Zhou N, Zhang J, Yi X, Wu D (2019) Hyaluronic acid-modified porous carbon-coated Fe_3O_4 nanoparticles for magnetic resonance imaging-guided photothermal/chemotherapy of tumors. Langmuir 35(40):13135–13144

Yang Y, Huang M, Qian J, Gao D, Liang X (2020) Tunable Fe_3O_4 nanorods for enhanced magnetic hyperthermia performance. Sci Rep 10(1):8331

Yonathan K, Mann R, Mahbub KR, Gunawan C (2022) The impact of silver nanoparticles on microbial communities and antibiotic resistance determinants in the environment. Environ Pollut 293:118506

Yu J, Zhao F, Gao W, Yang X, Ju Y, Zhao L, Guo W, Xie J, Liang XJ, Tao X (2019) Magnetic reactive oxygen species nanoreactor for switchable magnetic resonance imaging guided cancer therapy based on pH-sensitive Fe_5C_2@ Fe_3O_4 nanoparticles. ACS Nano 13(9):10002–10014

Zahran M, Marei AH (2019) Innovative natural polymer metal nanocomposites and their antimicrobial activity. Int J Biol Macromol 136:586–596

Zhao X, Tian R, Zhou J, Liu Y (2022) Multifunctional chitosan/grape seed extract/silver nanoparticle composite for food packaging application. Int J Biol Macromol 207:152–160